

Modeling and Numerical Simulation Of Tethered Buoy Dynamics [★]

Antonio Montano, ^a Marco Restelli, ^b Riccardo Sacco ^c

^a*Scientific Collaborator of MOX,
current affiliation: RSI Sistemi - Altran Group,
via A. de Togni 2, 20123 Milano*

^b*MOX - Modeling and Scientific Computing,
Dipartimento di Matematica “F. Brioschi”,
Politecnico di Milano, via Bonardi 9, 20133 Milano, Italy*

^c*Dipartimento di Matematica “F. Brioschi”,
Politecnico di Milano, via Bonardi 9, 20133 Milano, Italy*

Abstract

In this article we deal with the numerical simulation of the dynamics of a tethered buoy, which is a mechanical system for marine applications consisting of a rigid floating body (buoy) connected by an elastic cable to the bottom of the fluid environment. A novel mixed finite element formulation is proposed for the spatial numerical approximation of the equations governing the dynamics of the elastic cable. This is done to allow a robust modeling of the cable, even in the limit of an infinite value of the Young modulus, in a way that is similar to mixed formulations for incompressible fluid–mechanics. The dynamics of the floating body is described by the classical Euler equations of motion, written using quaternion variables to end up with a numerically robust algorithm in presence of large rotations. For the time discretization of the resulting coupled system of nonlinear differential equations, the Backward Euler implicit method is adopted due to the stability requirements of the problem at hand, while a damped Newton method is used for linearization. Finally, the accuracy and robustness of the proposed numerical procedure are validated in the simulation of the tethered buoy system under various static and dynamic working conditions.

Key words: Dynamical systems; mooring systems; finite element method; mixed formulations.

[★] This research activity was carried out at MOX - Modeling and Scientific Computing, Dipartimento di Matematica, Politecnico di Milano, Italy, within the Contract “*Sviluppo di un software per la simulazione della dinamica di boe e mede*”. Contractors: Politecnico di Milano - Dipartimento di Matematica and Resinex Trading S.r.l..

* Corresponding author: Riccardo Sacco

Email address: riccardo.sacco@mate.polimi.it (Riccardo Sacco).

1 Introduction

In this article we address the study of the dynamics of a tethered buoy, which is a mechanical system consisting of a rigid floating body (buoy) connected by an elastic cable to the bottom of the fluid environment. As an example of typical application, tethered buoy systems are developed to acquire and telemeter real-time data in atmospheric and oceanographic measurements during all seasons. Other relevant (and more conventional) uses of tethered buoys can be found in the design of signaling systems for navigation, or in station-keeping of large vessels (see Fig. 1). The problem under investigation has a highly complex fluid-structure interaction nature, so that it is expected that an accurate design of tethered buoys, for a wide range of applications as mentioned above, can benefit from a numerical simulation tool of the system under the action of several environmental loads.



Figure 1. An example of tethered buoy.

Let us give a brief summary of the contents of the article.

Section 2 deals with the main physical assumptions underlying the mathematical model of the two subsystems, the submerged cable and the floating body, and of the fluid environment (air and water) in which the moored system is moving. The second-order hyperbolic initial-boundary value problem for the submerged cable is presented in Sect. 2.2, while the classical Euler equations of motion for the dynamics of the floating body are discussed in Sect. 2.3. Quaternions are used as dependent variables because, unlike standard Euler angles, they do not exhibit singularities and are therefore well suited for a robust numerical solution of problems with large rotations, as the one considered in the present article (see [29,10,15]).

Section 3 deals with the discretization of the cable differential model. Concerning with spatial discretization, a novel mixed formulation of the cable differential model is proposed in Sects. 3.1-3.2 through the use of a Lagrangian multiplier which enforces in weak form the kinematical relation between displacement and strain. By doing so, the resulting weak model turns out to be robust and stable irrespectively of the value of the Young modulus E . In particular, the case of an

exactly inextensible cable is recovered by formally setting $E = +\infty$ in the constrained Hooke's law, in a completely analogous manner as is done to enforce the incompressibility constraint in mixed formulations for fluid–mechanical problems (see [12,9,4,5]). The accuracy and stability of the novel Galerkin mixed finite element approximation of the cable equation are then numerically demonstrated in Sect. 3.3.

The time discretization, the treatment of the coupling between the cable and buoy subsystems and the linearization of the whole coupled problem are the object of Section 4. Concerning with time discretization, the linear stability analysis carried out in Sect. 4.1 shows the practical impossibility of using an explicit time advancing method, due to an excessively small value of the resulting admissible time step. The full system of nonlinear ordinary differential algebraic equations describing the dynamics of the cable and of the floating body is summarized in Sect. 4.2.1 and advanced in time in Sect. 4.2.2 using the Backward Euler (BE) implicit scheme. The BE method is adopted due the ease of implementation and the reduced computational effort required to deal with long–time simulations, as is typically required in the industrial application at hand. The resulting nonlinear algebraic system of equations to be solved at each time step is then numerically solved using a damped Newton's method in Sect. 4.2.3.

The physical and numerical validation of the mathematical model and of the discretization algorithms discussed above are then carried out in Sect. 5, where the results obtained in the simulation of a tethered buoy under various static and dynamic working conditions are presented and discussed.

Finally, some concluding remarks and possible future extensions to the model and algorithms discussed in the article are addressed in Sect. 6.

2 Mathematical Model for the Dynamics of a Tethered Buoy

In this section, we describe the differential equations that constitute the mathematical model of a tethered buoy. This latter is a mechanical system composed by two coupled subsystems, an elastic cable representing the mooring device and a floating body (a buoy). The dynamics of the whole system is determined by the action of environmental loads, namely, forces due to surface waves, currents and wind [30,19,20,18], and of given external loads. In Sect. 2.1 we describe the above mentioned environmental loads; then, in the subsequent Sects. 2.2 and 2.3 we apply the model considered in Sect. 2.1 to the description of the dynamics of the cable and the buoy, respectively. The coupling between the two subsystems is deferred to Sect. 4.

2.1 Environmental Loads

In this section, we first address the mathematical model of fluid–structure interaction between water and an immersed body, and then we describe the drag forces due to the wind action.

Hydrodynamical loads acting on a body immersed in a marine environment consist of two terms, namely, added mass forces known from inviscid flow theory, and viscous drag forces produced by separation and boundary layer friction. The resulting force is a slight generalization of the so–called Morison’s equation [6], that is assumed to be valid when the body, or better its submerged part, is *slender*, i.e. when the *diffraction parameter* D_{max}/λ is less than 0.2, where λ and D_{max} denote the water wavelength and the maximum diameter of the body, respectively (see [27]). As for the contribution to hydrodynamical inertial forces due to surface waves, the slenderness assumption greatly simplifies the derivation of the Froude-Krilov force, due to the ambient and time-dependent pressure gradient, and of the disturbance force stemming from the interaction between waves and the solid body (see [19,30]). No contribution to inertial forces is instead accounted for by the action of the current, because the Keulegan–Carpenter number (which is a characteristic engineering parameter in marine applications) is very large in the case of a slender body [27].

Let \mathbf{v}_w and \mathbf{v}_c be the wave and current velocities, respectively, and \mathbf{v} denote the velocity of any point of the immersed body. Define also the ambient fluid velocity $\mathbf{v}_a = \mathbf{v}_w + \mathbf{v}_c$ and the *relative velocity* $\mathbf{v}_{rel} = \mathbf{v} - \mathbf{v}_a$. Moreover, let \mathbf{a} indicate the acceleration of any point of the immersed body and \mathbf{a}_w the acceleration of the fluid particles due to surface waves. Finally, let \mathbf{t} be the unit tangent vector of the slenderness axis of the body, and

$$\mathbf{n} = \frac{\mathbf{a}_w - (\mathbf{a}_w \cdot \mathbf{t})\mathbf{t}}{|\mathbf{a}_w - (\mathbf{a}_w \cdot \mathbf{t})\mathbf{t}|}$$

be the unit normal vector which lies on the plane univocally identified by \mathbf{t} and \mathbf{a}_w . Then, the added mass force per unit length \mathbf{f}_{am} and the normal and tangential drag forces per unit length \mathbf{f}_{dn} and \mathbf{f}_{dt} can be expressed by the following *generalized Morison’s equation*

$$\begin{aligned} \mathbf{f}_{am} &= \rho_w A [C_M |\mathbf{a}_w \cdot \mathbf{n}| - (C_M - 1) |\mathbf{a} \cdot \mathbf{n}|] \mathbf{n} \\ \mathbf{f}_{dt} &= -\frac{1}{2} C_{dt} \rho_w D |\mathbf{v}_{rel} \cdot \mathbf{t}| (\mathbf{v}_{rel} \cdot \mathbf{t}) \mathbf{t} \\ \mathbf{f}_{dn} &= -\frac{1}{2} C_{dn} \rho_w D |\mathbf{v}_{rel} - (\mathbf{v}_{rel} \cdot \mathbf{t})\mathbf{t}| (\mathbf{v}_{rel} - (\mathbf{v}_{rel} \cdot \mathbf{t})\mathbf{t}), \end{aligned} \tag{1}$$

where C_M , C_{dt} and C_{dn} are added mass and drag coefficients. The quantities ρ_w , A and D denote the fluid density, and a characteristic cross-section and diameter of

the body, respectively.

Wind effect is given through its velocity profile. Denoting by \mathbf{v}_{wind} the wind velocity vector and by v_{10} the wind speed at $10m$ above the sea surface, the strength of the local wind velocity at z meters above the sea surface can be expressed by $|\mathbf{v}_{wind}| = v_{10}(z/10)^{1/7}$, so that the wind force acting on the floating body is

$$\mathbf{F}^{wind} = \frac{1}{2} C_{wind} \rho_{air} A_T |\mathbf{v}_{wind}| \mathbf{v}_{wind}, \quad (2)$$

where ρ_{air} is the air density, A_T is the floating body cross-section along the wind direction and C_{wind} is a suitable coefficient derived from experiments [7].

2.2 Cable Model

In this section, we describe the mathematical model governing the dynamics of the submerged cable under the assumption of negligible bending and torsional stiffness. This is a reasonable approximation of the behaviour of a long steel-made cable for marine offshore applications [1]. Let T and \mathbf{r} be the tension and displacement of any point of an extensible cable of unstretched length L , cross-section A_0 and linear density ρ_0 . We also indicate by s the curvilinear abscissa along the unstretched cable and let

$$e = \left| \frac{\partial \mathbf{r}}{\partial s} \right| - 1 \quad (3)$$

denote the strain of the cable itself. The cable dynamics is expressed by the following second-order hyperbolic equation

$$\rho_0 \frac{\partial^2 \mathbf{r}}{\partial t^2} = \frac{\partial}{\partial s} \left(\frac{T}{1+e} \frac{\partial \mathbf{r}}{\partial s} \right) + \mathbf{f}(1+e), \quad (4)$$

where T and \mathbf{r} are functions of s and t , with $s \in [0, L]$ and $t \in \mathcal{I}_{t_{fin}} \equiv (0, t_{fin}]$, t_{fin} being the final time of integration, while \mathbf{f} is the sum of all external forces per unit stretched length. To complete the mathematical model (4), a constitutive relation for T and an explicit expression of the force term must be provided. As for the tension T , Hooke's law is assumed to hold

$$T = E A_0 e, \quad (5)$$

relating strain and tension through the Young modulus E . As for the external hydrodynamical forces, a submerged cable is subject to:

- gravity and hydrostatic forces $\mathbf{f}_{hg} = \rho_0(\rho_c - \rho_w)/((1+e)\rho_c)\mathbf{g}$, where \mathbf{g} is gravity acceleration and ρ_c, ρ_w are cable and water densities, respectively;

- hydrodynamic inertia force \mathbf{f}_{am} given by equation (1)₁, which physically corresponds to an increased mass effect for cable dynamics;
- normal and tangential hydrodynamic drag forces \mathbf{f}_{dn} and \mathbf{f}_{dt} , that can be properly computed by considering normal and tangential directions in the generalized Morison's equation (1)₂ and (1)₃.

The above contributions are to be intended as forces per unit stretched length, and must be summed up to give

$$\mathbf{f} = \mathbf{f}_{hg} + \mathbf{f}_{am} + \mathbf{f}_{dn} + \mathbf{f}_{dt}. \quad (6)$$

Substituting (5) and (6) into (4), yields the following second-order hyperbolic initial-boundary value problem: find $\mathbf{r} = \mathbf{r}(t, s)$ such that

$$\left\{ \begin{array}{l} \rho_0 \frac{\partial^2 \mathbf{r}}{\partial t^2} = \frac{\partial}{\partial s} \left(E A_0 \frac{e}{1+e} \frac{\partial \mathbf{r}}{\partial s} \right) + (1+e)(\mathbf{f}_{hg} + \mathbf{f}_{am} + \mathbf{f}_{dn} + \mathbf{f}_{dt}), \\ s \in (0, L), \quad t \in \mathcal{I}_{t_{fin}} \\ \mathbf{r}(t, 0) = \mathbf{0}, \quad \mathbf{r}(t, L) = \mathbf{r}_{bnd}(t), \quad \forall t \in \overline{\mathcal{I}_{t_{fin}}} \\ \mathbf{r}(0, s) = \mathbf{r}_0(s), \quad \dot{\mathbf{r}}(0, s) = \mathbf{v}_0(s), \end{array} \right. \quad (7)$$

where $\mathbf{0} = [0, 0, 0]^T$, and for any time level t , the vector quantity $\mathbf{r}_{bnd}(t)$ is a Dirichlet boundary datum provided by the coupling between cable and floating body, while \mathbf{r}_0 and \mathbf{v}_0 are suitable initial conditions.

2.3 Floating Body Model

In this section, we describe the Euler equations governing the motion of the buoy. As anticipated in the Introduction, quaternions are used as rotational degrees of freedom because they do not exhibit singularities in presence of large rotations. Sect. 2.3.1 illustrates the Euler equations for the buoy dynamics while in Sect. 2.3.2 the loads acting on the buoy itself are derived from the general framework discussed in Sect. 2.1.

2.3.1 Motion equations of the floating buoy

Let $\mathbf{r}_C = \mathbf{r}_C(t)$, M_b and \mathcal{I}_C denote the position of the center of mass C , the mass and inertia tensor about the center of mass of the buoy, respectively. Moreover, let $\mathbf{q}_4 = \mathbf{q}_4(t) = [q_0, \mathbf{q}]^T \in \mathbb{R}^4$, with $q_0 \in \mathbb{R}$ and $\mathbf{q} \in \mathbb{R}^3$, be the unit quaternion representing the orientation of the buoy with respect to a fixed reference configuration (see [10] and [15]). Finally, in order to write the Euler equations of motion as a first-order system of ordinary differential equations (ODE) we also introduce

the state variables \mathbf{p} and \mathbf{L}_C , representing the linear momentum and the angular momentum about C , respectively. Then, the Euler equations of motion read

$$\begin{cases} \dot{\mathbf{r}}_C = M_b^{-1} \mathbf{p} \\ \dot{\mathbf{p}} = \mathbf{F} \\ \dot{\mathbf{q}}_4 = \frac{1}{2} \mathbf{Q}(\mathcal{I}_C^{-1} \mathbf{L}_C) \circ \mathbf{q}_4 \\ \dot{\mathbf{L}}_C = \boldsymbol{\tau}_C, \end{cases} \quad (8)$$

where \mathbf{F} and $\boldsymbol{\tau}_C$ are forces and torques acting on the rigid-body, \mathbf{Q} is a prolongation operator defined as

$$\begin{aligned} \mathbf{Q} : \mathbb{R}^3 &\rightarrow \mathbb{R}^4 \\ \mathbf{v} &\mapsto [0, \mathbf{v}]^T \equiv \mathbf{v}_4 \end{aligned}$$

and the product between the quaternions \mathbf{v}_4 and \mathbf{u}_4 is defined as

$$\mathbf{v}_4 \circ \mathbf{u}_4 = \begin{bmatrix} v_0 u_0 - \mathbf{v} \cdot \mathbf{u} \\ v_0 \mathbf{u} + u_0 \mathbf{v} + \mathbf{v} \times \mathbf{u} \end{bmatrix},$$

where the symbols \cdot and \times denote the usual scalar and vector products in \mathbb{R}^3 , respectively. System (8), supplemented by suitable initial conditions, can in principle be integrated in the time interval $\mathcal{I}_{t_{fin}}$, to compute the dynamics of the rigid body. Still, when considering the dynamics of the coupled system composed by the buoy and the mooring cable, it is necessary to track the position of the mooring point, which leads to introducing further variables and corresponding kinematical constraints. Thus, let β and $\boldsymbol{\lambda}$ be the Euler parameters associated with \mathbf{q}_4 such that $q_0 = \cos(\beta/2)$ and $\mathbf{q} = \boldsymbol{\lambda} \sin(\beta/2)$ and let

$$R(\mathbf{q}_4) = [\cos(\beta)I + (1 - \cos(\beta))\boldsymbol{\lambda}\boldsymbol{\lambda}^T + \sin(\beta)S(\boldsymbol{\lambda})] \in \mathbb{R}^{3 \times 3},$$

be the corresponding rotation matrix, where $S(\boldsymbol{\lambda}) \in \mathbb{R}^{3 \times 3}$ denotes the skew-symmetric tensor associated with $\boldsymbol{\lambda}$. Denoting by \mathbf{r}_O the unknown position of the mooring point and by \mathbf{r}_{CO}^0 the vector $\mathbf{r}_O(0) - \mathbf{r}_C(0)$, which connects points C and O in the reference configuration, the rigid body constraint provides

$$\mathbf{r}_O - R(\mathbf{q}_4) \mathbf{r}_{CO}^0 - \mathbf{r}_C = \mathbf{0} \quad \forall t \in \mathcal{I}_{t_{fin}}. \quad (9)$$

2.3.2 Forces and torques acting on the floating buoy

In this section, we describe the forces \mathbf{F} and torques $\boldsymbol{\tau}_C$ (these latter being evaluated with respect to the center of mass C) introduced in (8). We distinguish among the following contributions:

- restoring force (Archimede's force), \mathbf{F}^r ;
- additional forces due to marine environment, \mathbf{F}^{hyd} ;
- wind effect, \mathbf{F}^{wind} ;
- force exerted by the cable, \mathbf{F}^c ;
- given external forces (station keeping traction), \mathbf{F}^{ext} ,

and obtain the resulting force \mathbf{F} as the sum of these contributions. Clearly, a similar classification applies also to the corresponding torques. In the following, we indicate by $\mathbf{r}_{BC} = \mathbf{r}_{BC}(t)$ and $M_D = M_D(t)$ the position of the buoyancy center and the fluid displaced mass by the floating body at time t , respectively. Kinematical components \mathbf{v}_{BC} and \mathbf{a}_{BC} at the buoyancy center (considered as a point belonging to the solid buoy) can be computed via standard rigid body kinematical relations. The mathematical expressions of the forces then read

$$\left\{ \begin{array}{l} \mathbf{F}^r = (M_b - M_D)\mathbf{g} \\ \mathbf{F}^{hyd} = M_D [C_M \mathbf{a}_w(\mathbf{r}_{BC}) - (C_M - 1)\mathbf{a}_{BC}] \\ \quad - \frac{1}{2} C_{dn} \rho_w H_{sub} \langle D_{sub} \rangle |\mathbf{v}_{rel} - (\mathbf{v}_{rel} \cdot \mathbf{t})\mathbf{t}| (\mathbf{v}_{rel} - (\mathbf{v}_{rel} \cdot \mathbf{t})\mathbf{t}) \\ \mathbf{F}^{wind} = \frac{1}{2} C_{wind} \rho_{air} A_T |\mathbf{v}_{wind}| \mathbf{v}_{wind} \\ \mathbf{F}^c = \mathbf{T}_O \\ \mathbf{F}^{ext} = \mathbf{F}^{tr}. \end{array} \right. \quad (10)$$

In (10)₁, $\mathbf{g} = [0, 0, -9.81]^T m s^{-2}$ is the gravity acceleration. Eq. (10)₂ is obtained integrating (1) along the axis of the buoy, setting $\mathbf{v}_{rel} = \mathbf{v}_{BC} - \mathbf{v}_a(\mathbf{r}_{BC})$ and denoting by H_{sub} and $\langle D_{sub} \rangle$ the height and a representative diameter of the submerged portion of the buoy, respectively. Eq. (10)₃ is nothing but (2). Finally, \mathbf{T}_O in (10)₄ is the traction exerted by the cable and \mathbf{F}^{tr} in (10)₅ is a known datum. The mathematical expressions of the torques corresponding to (10) read

$$\left\{ \begin{array}{l} \boldsymbol{\tau}_C^r = (\mathbf{r}_{BC} - \mathbf{r}_C) \times (-M_D \mathbf{g}) \\ \boldsymbol{\tau}_C^{hyd} = (\mathbf{r}_{BC} - \mathbf{r}_C) \times \mathbf{F}^{hyd} \\ \boldsymbol{\tau}_C^{wind} = (\mathbf{r}_{wind} - \mathbf{r}_C) \times \mathbf{F}^{wind} \\ \boldsymbol{\tau}_C^c = (\mathbf{r}_O - \mathbf{r}_C) \times \mathbf{T}_O \\ \boldsymbol{\tau}_C^{ext} = (\mathbf{r}_{ext} - \mathbf{r}_C) \times \mathbf{F}^{ext} \end{array} \right.$$

where \mathbf{r}_{wind} and \mathbf{r}_{ext} are the position vectors of the points of application of \mathbf{F}^{wind} and \mathbf{F}^{ext} , respectively. Concerning the expression of $\boldsymbol{\tau}_C^{hyd}$, we observe that this quantity is computed using a suitable extension of the classical theory that is rigorously valid for cylindrical bodies (see [17,30]). In particular, since no explicit

(or easily computable) relation is available for the point of application of \mathbf{F}^{hyd} , we assume for simplicity that it coincides with the buoyancy center.

3 Numerical Approximation of the Cable Dynamics Problem

In this section, we deal with the spatial numerical approximation of the cable initial-boundary value system (7). With this aim, a novel mixed formulation of the differential model is introduced in Sect. 3.1 through the use of a Lagrange multiplier (tension) which enforces in weak form the kinematical relation between displacement and strain. This provides a robust modeling of the cable, because no singularity arises in the displacement–strain relation even in the limit of an infinite value of the Young modulus. Moreover, the introduction of the above mixed variable avoids the onset of possible numerical instabilities in the computation of the tension along the cable length. This approach is analogous to mixed formulations for incompressible fluid–mechanics where the incompressibility constraint is enforced through the use of the pressure parameter (see [12,9,4,5]). The Galerkin finite element spatial discretization of the mixed weak formulation of (7) is addressed in Sect. 3.2, while in Sect. 3.3 an extensive validation of the stability and accuracy of the method are carried out in the numerical simulation of a stationary test case for which an exact solution is available.

3.1 Mixed Weak Formulation for Cable Dynamics

In this section, we introduce a novel mixed weak formulation for the cable dynamics system (7). For ease of presentation, we assume that the source term \mathbf{f} and the boundary tension \mathbf{T}_{bnd} are given functions. Let

$$V = \left\{ \mathbf{v} \in (H^1(0, L))^3 \mid v(0) = 0 \right\}, \quad Q = L^2(0, L),$$

and denote by $(f, g) = \int_0^L f g ds$ the standard L^2 inner product for every $f, g \in L^2(0, L)$. Then, the mixed weak formulation of (7) reads:

for every $t \in \mathcal{I}_{t_{fin}}$, find $\mathbf{r} \in V$ and $T \in Q$ such that

$$\begin{cases} \rho_0 \left(\frac{\partial^2 \mathbf{r}}{\partial t^2}, \mathbf{v} \right) + \left(\frac{T}{1+e} \frac{\partial \mathbf{r}}{\partial s}, \frac{\partial \mathbf{v}}{\partial s} \right) = ((1+e) \mathbf{f}, \mathbf{v}) + \mathbf{T}_{bnd} \cdot \mathbf{v}(L) & \forall \mathbf{v} \in V \\ \left(\frac{1}{1+e} \left| \frac{\partial \mathbf{r}}{\partial s} \right|^2, q \right) = ((1+e), q) & \forall q \in Q, \end{cases} \quad (11)$$

where, according to (5), we have

$$e = e(T) = \frac{T}{E A_0}. \quad (12)$$

Problem (11) is a weak formulation subject to the extensibility constraint for the cable, that can be conveniently treated with a *mixed* approach, i.e., a method where two independent variables, \mathbf{r} and T , are simultaneously present. Precisely, $(11)_1$ is Newton's law in weak form (i.e., after integration by parts of $(7)_1$), $(11)_2$ is the weak form of the kinematical relation (3) and (12) is just Hooke's law.

It is interesting to notice that when $E = +\infty$ there is a strong analogy between the mixed formulation (11) and mixed formulations for incompressible fluid-mechanics (see [12,9,4,5]). As a matter of fact, letting $\lambda = E A_0$, Hooke's law can be written as $e = T/\lambda$, and the case of an *inextensible* cable can be obtained by setting $\lambda = +\infty$. In the same manner, denoting again by λ the second Lamè coefficient for an elastic material, and by p the pressure parameter, the case of an *incompressible* material (which corresponds to the case of an incompressible fluid in creeping flow problems, Stokes problem) can be obtained by setting $\lambda = +\infty$ in the relation $p/\lambda = -\text{div } \mathbf{u}$, \mathbf{u} being the displacement (velocity) vector field.

3.2 Mixed Finite Element Approximation for Cable Dynamics

In this section, we construct the finite element approximation of (11) using the Galerkin method. Let \mathcal{T}_h be a given partition of $[0, L]$ into N_h subintervals K of uniform length $H = L/N_h$. Let μ and ν be given integers, with $\mu \geq 1$ and $0 \leq \nu < \mu$. We introduce the following finite element spaces defined over \mathcal{T}_h

$$\begin{aligned} V_h &= \{\mathbf{v}_h \in V \mid \mathbf{v}_h \in (\mathbb{P}_\mu(K))^3 \ \forall K \in \mathcal{T}_h\}, \\ Q_h &= \{q_h \in Q \mid q_h \in \mathbb{P}_\nu(K) \ \forall K \in \mathcal{T}_h\}. \end{aligned} \quad (13)$$

Then, the Galerkin finite element approximation of (11) reads:

for every $t \in \mathcal{I}_{t_{fin}}$, find $\mathbf{r}_h \in V_h$ and $T_h \in Q_h$ such that

$$\left\{ \begin{aligned} \rho_0 \left(\frac{\partial^2 \mathbf{r}_h}{\partial t^2}, \mathbf{v}_h \right) + \left(\frac{T_h}{1 + e_h} \frac{\partial \mathbf{r}_h}{\partial s}, \frac{\partial \mathbf{v}_h}{\partial s} \right) \\ = ((1 + e_h) \mathbf{f}, \mathbf{v}_h) + \mathbf{T}_{bd,h} \cdot \mathbf{v}_h(L) & \quad \forall \mathbf{v}_h \in V_h \\ \left(\frac{1}{1 + e_h} \left| \frac{\partial \mathbf{r}_h}{\partial s} \right|^2, q_h \right) = ((1 + e_h), q_h) & \quad \forall q_h \in Q_h \end{aligned} \right. \quad (14)$$

with $e_h = T_h/(E A_0)$.

Different choices of the polynomial degrees for V_h and Q_h in (13) and the corresponding impact on the accuracy of the approximation will be extensively addressed in the numerical experiments shown in Sect. 3.3. In order to construct explicit expressions for the finite element equation to be solved numerically, we denote by $\mathbf{r}_i(t)$ and $T_l(t)$ the degrees of freedom for \mathbf{r}_h and T_h , respectively, with $i = 1, \dots, N_{h_r}$ and $l = 1, \dots, N_{h_T}$. Moreover, for any vector $\mathbf{p} \in \mathbb{R}^3$ we let p^k indicate its k -th cartesian component. Then, we obtain the following system of ordinary differential algebraic equations (ODAE), for $i, j, s = 1, \dots, N_{h_r}$, $l, p = 1, \dots, N_{h_T}$ and $k = 1, 2, 3$

$$\begin{cases} \frac{1}{6}\rho_0 H^2 m_{ij} \ddot{r}_j^k = -K_{ijp} T_p r_j^k + H T_{bnd}^k \varphi_i(L) + H^2 f_i^k \\ 0 = -\frac{1}{2}K_{jst} r_j^k r_s^k + \frac{1}{2}H^2 d_l, \end{cases} \quad (15)$$

where summation over repeated indices is understood and

$$\begin{aligned} m_{ij} &= \frac{6}{H} (\varphi_j, \varphi_i), & K_{ijp} &= H \left(\frac{d\varphi_j}{ds} \frac{d\varphi_i}{ds}, \frac{\psi_p}{1+e_h} \right), \\ f_i^k &= \frac{1}{H} \left((1+e_h) f^k, \varphi_i \right), & d_l &= \frac{1}{H} \left((1+e_h), \psi_l \right), \end{aligned} \quad (16)$$

having denoted by $\varphi_i \in \mathbb{P}_\mu$ and $\psi_i \in \mathbb{P}_\nu$ the scalar basis functions for V_h and Q_h , respectively. We notice that the factor $1/2$ in the right-hand side of (15)₂ has been added to end up with a symmetric formulation after linearization of system (15). In view of the time discretization of (15), it is convenient to rewrite the problem as a first-order ordinary differential system by introducing an auxiliary velocity variable v . This yields the following system, for $i, j, s, q = 1, \dots, N_{h_r}$, $l, p = 1, \dots, N_{h_T}$ and $k = 1, 2, 3$

$$\begin{cases} \dot{r}_q^k = v_q^k \\ \frac{1}{6}\rho_0 H^2 m_{ij} \dot{v}_j^k = -K_{ijp} T_p r_j^k + H T_{bnd}^k \varphi_i(L) + H^2 f_i^k \\ 0 = -\frac{1}{2}K_{jst} r_j^k r_s^k + \frac{1}{2}H^2 d_l. \end{cases} \quad (17)$$

Time integration of the ODAE system (17) and linearization of the resulting non-linear system of algebraic equations will be discussed in Sect. 4.

3.3 The mixed formulation in the stationary case

In this section, we first carry out the linearization of the mixed formulation (11) in the stationary case. This case, besides being of interest by its own, is also a crucial step within the discretization of the complete time-dependent problem. Then, we perform extensive numerical experiments to validate the accuracy and stability of

the corresponding Galerkin approximation using the finite element spaces (13), in the simulation of a test problem for which an analytical solution is available.

3.3.1 Linearization using the Newton method

For ease of presentation, we study the case of a mooring system composed by an inextensible cable ($E = +\infty$ in (11), which implies $e = 0$), subject to a prescribed position at the end points and to a given force term $\mathbf{f} = \mathbf{f}(s)$. When considering a real cable, with a large but finite value of E , we expect that $e \ll 1$, which allows us to assume e to be constant in the linearization of (11), in such a way that the treatment of this section still applies. The nonlinear boundary value problem modeling the tension and the position vector of any point of the system reads

$$\begin{cases} -\frac{\partial}{\partial s} \left(T \frac{\partial \mathbf{r}}{\partial s} \right) = \mathbf{f} \\ \frac{1}{2} \left(\left| \frac{\partial \mathbf{r}}{\partial s} \right|^2 - 1 \right) = 0 \\ \mathbf{r}(0) = \mathbf{0}, \quad \mathbf{r}(L) = \mathbf{g}. \end{cases} \quad \text{in } \Omega_s = (0, L) \quad (18)$$

The Newton linearization of (18) in the neighbourhood of a given cable configuration $(\bar{\mathbf{r}}, \bar{T})$ is

$$\begin{cases} -\frac{\partial}{\partial s} \left(\bar{T} \frac{\partial \mathbf{w}}{\partial s} \right) - \frac{\partial}{\partial s} \left(u \frac{\partial \bar{\mathbf{r}}}{\partial s} \right) = - \left(-\frac{\partial}{\partial s} \left(\bar{T} \frac{\partial \bar{\mathbf{r}}}{\partial s} \right) - \mathbf{f} \right) \\ \frac{\partial \bar{\mathbf{r}}}{\partial s} \cdot \frac{\partial \mathbf{w}}{\partial s} = -\frac{1}{2} \left(\left| \frac{\partial \bar{\mathbf{r}}}{\partial s} \right|^2 - 1 \right) \\ \mathbf{w}(0) = \mathbf{w}(L) = \mathbf{0}, \end{cases} \quad \text{in } \Omega_s \quad (19)$$

where $\mathbf{w} = \mathbf{w}(s)$ and $u = u(s)$ are the Newton variations associated with \mathbf{r} and T , respectively. Letting $V = (H_0^1(\Omega_s))^3$, the weak form of system (19) is readily obtained as: find $\mathbf{w} \in V$, $u \in Q$ such that, for all $\mathbf{v} \in V$ and $q \in Q$, we have

$$\begin{cases} \left(\bar{T} \frac{\partial \mathbf{w}}{\partial s}, \frac{\partial \mathbf{v}}{\partial s} \right) + \left(u, \frac{\partial \bar{\mathbf{r}}}{\partial s} \cdot \frac{\partial \mathbf{v}}{\partial s} \right) = - \left[\left(\bar{T}, \frac{\partial \bar{\mathbf{r}}}{\partial s} \cdot \frac{\partial \mathbf{v}}{\partial s} \right) - (\mathbf{f}, \mathbf{v}) \right] \\ \left(q, \frac{\partial \bar{\mathbf{r}}}{\partial s} \cdot \frac{\partial \mathbf{w}}{\partial s} \right) = -\frac{1}{2} \left[\left(q, \left| \frac{\partial \bar{\mathbf{r}}}{\partial s} \right|^2 \right) - (q, 1) \right]. \end{cases} \quad (20)$$

The linearized system (20) can be written in the form of a saddle–point problem as

$$\begin{pmatrix} A & B^T \\ B & 0 \end{pmatrix} \begin{pmatrix} \mathbf{w} \\ u \end{pmatrix} = \begin{pmatrix} F \\ G \end{pmatrix}, \quad (21)$$

where, denoting by V' and Q' the dual spaces of V and Q , respectively, we have introduced the operators $A \in \mathcal{L}(V; V')$, $B \in \mathcal{L}(V; Q')$ and its adjoint operator $B^T \in \mathcal{L}(Q; V')$, and the right hand sides $F \in V'$, $G \in Q'$, $\mathcal{L}(X; Y)$ being the space of linear and continuous functionals from X into Y (see [2,23]). Notice that the discrete counterparts of the operators A and B in (21) can be readily obtained from the quantities K_{ijp} in (16). The analysis of well-posedness for the linearized saddle–point problem (20), as well as the convergence analysis of the corresponding Galerkin finite element approximation, will be the object of a subsequent article. In the nextcoming section, we provide an extensive numerical validation of the method, using the finite element spaces (13).

3.3.2 Numerical validation of the mixed formulation

In this section, we illustrate the results obtained in the simulation of a three-dimensional mooring system for which a closed–form solution for the cable point position and tension is available [13]. We refer to [1,24] for further comparison with different discretization approaches. In all numerical experiments, we assume that the cable has unit length L and density ρ_0 , and that the external force \mathbf{f} acting on the cable is its weight. As for the boundary conditions, we consider the cases where Dirichlet or Neumann data are imposed at $s = L$, while we always assume $\mathbf{r}(0) = \mathbf{0}$. Finally, we point out that in all the computations the strain e is replaced by the piecewise constant function over \mathcal{T}_h defined as $\bar{e}_i = \bar{T}_i / (E A_0)$, where \bar{T}_i is the average tension on the i -th mesh element, which considerably simplifies the evaluation of the quantities in (16). As will be shown below, this does not sensibly affect the accuracy of the scheme in the case of near-inextensible cable materials (for which the assumption $e \simeq 0$ is reasonable), while it produces a significant spoiling of the performance of the method if the cable extensibility is large.

The first two examples are concerning with optimal combinations of the polynomial degrees μ and ν in (13), with $k = 1, \dots, 4$. In the first numerical experiment, we assume a Neumann boundary condition for the tension at $s = L$ and we consider an inextensible cable ($E A_0 = +\infty$). The results of the simulation are summarized in Fig. 2, which shows the L^2 (left) and H^1 (right) norms of the error associated with the position vector, as a function of h and for the several values of k . Completely similar results are obtained for the error on the tension variable. The resulting convergence rates for both variables agree with the optimal theoretical estimates for primal mixed formulations which predict $\mathcal{O}(h^k)$ convergence in H^1 for the position variable and $\mathcal{O}(h^k)$ convergence in L^2 for the stress variable, corresponding to the cable tension variable in the problem at hand (see [26], Chapt.IV).

The same problem as before is solved assuming to deal with an extensible cable, where $E A_0$ is such that the stretching of the cable is of the order of 50 percent of its length. The results of the simulation are summarized in Fig. 3. On the left–hand side of the figure, the error curves (in the L^2 and H^1 norms) associated with

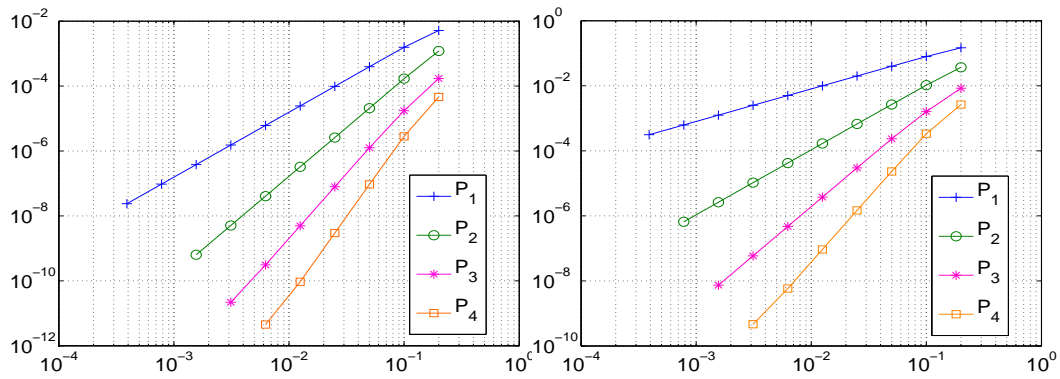


Figure 2. Error curves for the position vector. Left: L^2 norm. Right: H^1 norm. The value of $E A_0$ is $+\infty$.

the position variable are plotted as a function of the mesh size h for the various values of k . It is clearly visible that the accuracy of the method is spoiled by the approximate treatment of the extensibility. On the right-hand side, the error curves (in the L^2 norm) associated with the tension variable are plotted as a function of the mesh size h for the various values of k . In this case, the computed convergence rates agree with the optimal theoretical estimates.

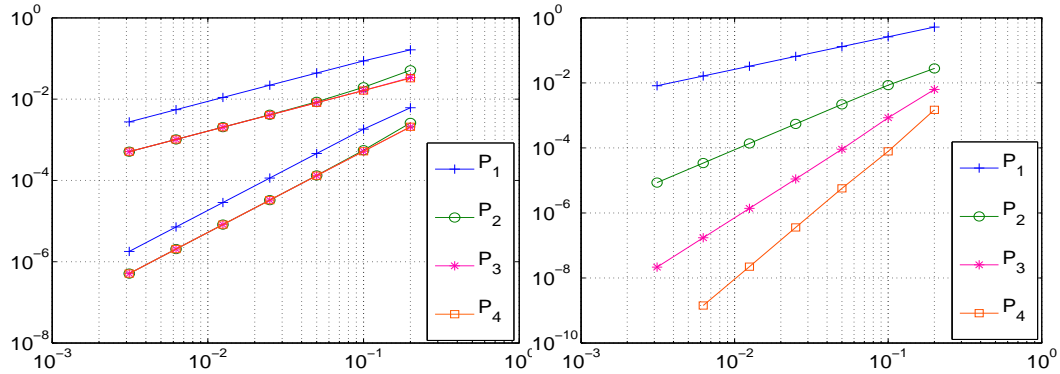


Figure 3. Left: error curves for the position vector (L^2 and H^1 norms). Right: error curves for the tension (L^2 norm).

The next two examples are concerning with non-optimal combinations of the polynomial degrees μ and ν . In the first test case, we assume $E A_0 = +\infty$ and set $\mu = 4$, $\nu = 0, \dots, 3$. Fig. 4 shows the error curves associated with the position variable, in L^2 norm (left) and H^1 norm (right), as a function of h and for the various values of ν . It is clearly seen that the convergence rates maintain their optimality, according with the polynomial degree chosen for the tension variable (i.e., $\mathcal{O}(h^{\nu+1})$ for the H^1 norm of the error, and $\mathcal{O}(h^{\nu+2})$ for the L^2 norm of the error). Similar results are obtained for the error on the tension variable.

In spite of the degradation of the order of the scheme shown in the previous case, the use of non-optimal combinations of the polynomial degrees can be attractive when coarse discretization are considered, as demonstrated by the next test case. Here, we consider the “rising” of the end point of the cable from the position

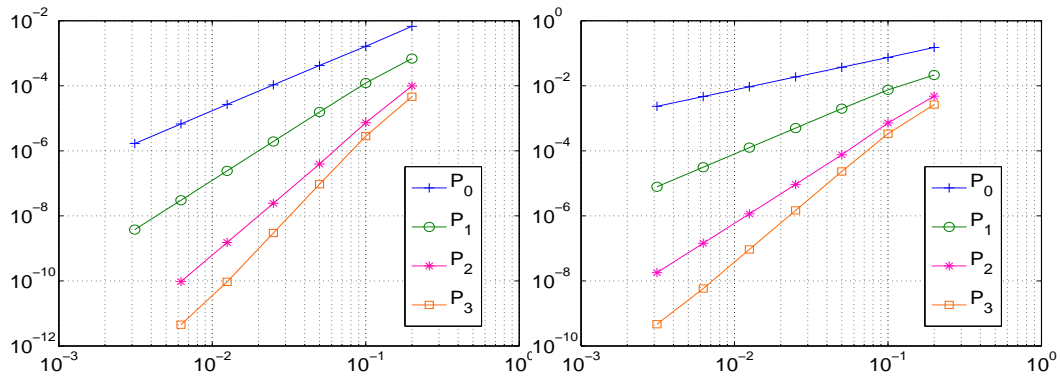


Figure 4. Error curves for the position vector. Left: L^2 norm. Right: H^1 norm. The value of λ is $+\infty$, while $\mu = 4$ and $\nu \in [0, 3]$.

$\mathbf{g}_a = [0.01, 0, 0.8]$ to the final position $\mathbf{g}_b = [0.01, 0, 0.99]$ and we compare two spatial discretizations: the first one consists of 10 elements with $\mu = 1, \nu = 0$ (optimal combination), while the second one consists of 5 elements with $\mu = 2, \nu = 0$ (non-optimal combination). In both cases we have the same number of degrees of freedom for the position variable. Results are shown in Fig.5. The \mathbb{P}_1 - \mathbb{P}_0 elements behave as rigid beams, thus causing large non-physical horizontal position vectors and negative tensions. On the other hand, the more flexible \mathbb{P}_2 - \mathbb{P}_0 elements can capture the correct profile of the cable. In particular, we notice the extremely varying horizontal scales in the two figures and also the fact that the semi-circular bending of the cable around $s = 0$ is resolved within one mesh element when the space \mathbb{P}_2 - \mathbb{P}_0 is used (Fig. 5, right).

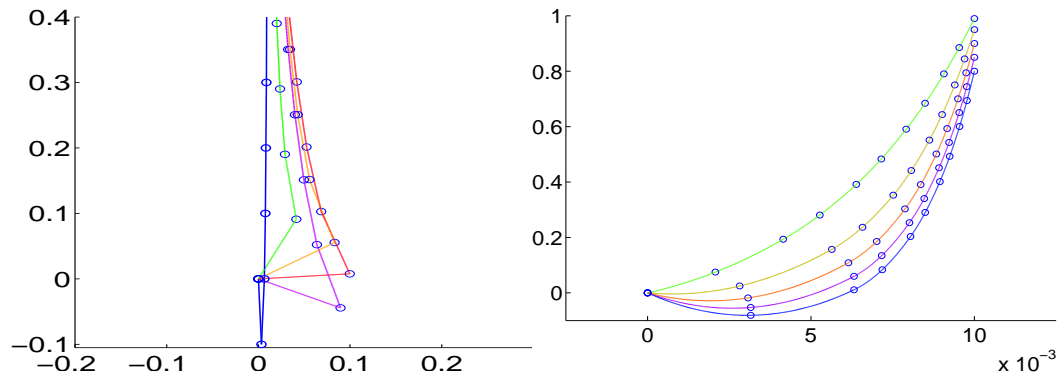


Figure 5. The “rising” of the end point of the cable from $\mathbf{g}_a = [0.01, 0, 0.8]$ to $\mathbf{g}_b = [0.01, 0, 0.99]$. Left: ten \mathbb{P}_1 - \mathbb{P}_0 elements, behaving as rigid beams. Right: five \mathbb{P}_2 - \mathbb{P}_0 elements.

4 Time Discretization, Coupling Algorithm and Linearization

In this section, we address in detail the main issues in the numerical modeling of the dynamics of the tethered buoy system, viz, its time discretization, the procedure

to couple the two subsystems (cable and floating body) and the linearization of the resulting nonlinear algebraic system through a properly damped Newton's method.

Concerning with the time discretization of the problem, the linear stability analysis of Sect. 4.1 for the equations describing the cable dynamics shows the practical impossibility of using an explicit time advancing method. The admissible time step, in fact, would be excessively small when dealing with long-time simulations, as is typically required in the industrial application at hand. As a consequence, the adoption of an implicit scheme is necessary. Our choice falls on the implicit Backward Euler (BE) scheme (see Sect. 4.2.2) because of the robustness and ease of implementation of the method, and its ability to handle in a straightforward manner the differential-algebraic equations governing the coupled system. For a different discretization strategy, using piecewise linear continuous finite elements for the spatial approximation of position and velocity, and a Runge-Kutta explicit fourth-order scheme for time advancing, we refer to [1].

Concerning with the coupling between the two subsystems, two main strategies can be employed, namely, a staggered (or decoupled) approach or a fully coupled approach. In the first case, a suitable numerical splitting of the two subsystems is carried out in order to end up with efficient algorithms in presence of a high number of degrees of freedom. In the second case, on the contrary, the complete system is treated within a monolithic framework, this of course being more computationally demanding but with the advantage of providing a more robust and stable treatment of the nonlinearity. In our specific context, the number of degrees of freedom associated with the buoy is negligible with respect to those of the cable, so that no appreciable efficiency gain is expected in using a staggered algorithm. Therefore, a fully coupled approach is adopted, as explained in Sect. 4.2.1, and the linearization of the nonlinear algebraic system of equations resulting from time advancing with the BE scheme is numerically carried out at each time step using a properly damped Newton's method as described in Sect. 4.2.3.

4.1 *Linear stability analysis*

In this section we carry out a stability analysis for a simple linear differential model problem associated with the cable equation (22), following the classical guideline of [28,12,31]. With this aim, let us consider the dynamics of a cable with no applied loads and assume a rectilinear initial configuration. It is easy to see that the cable remains rectilinear during its motion, so that we can set $\mathbf{r} = [r_x, 0, 0]^T$. Moreover, equation (4) turns out to be linear and, denoting by $u = r_x - s$ the (one-dimensional) displacement with respect to the unstretched configuration, we get the

following model

$$\rho_0 \frac{\partial^2 u}{\partial t^2} = \frac{\partial}{\partial s} \left(E A_0 \frac{\partial u}{\partial s} \right). \quad (22)$$

Assuming to employ a uniform partition of the interval $\overline{\Omega}_s$ into elements Ω_e of width $H = L/N_h$, the standard \mathbb{P}_1 -finite element semi-discretization of (22) leads to solving the following system of second-order ordinary differential equations

$$M \frac{d^2 \mathbf{u}}{dt^2} = K \mathbf{u}, \quad (23)$$

where M and K are the mass matrix and stiffness matrix, respectively. Denoting by $M^{(e)}$ and $K^{(e)}$ the element matrices associated with the discrete scheme, the eigenvalues of $M^{(e)}$ are $\lambda_{1,2} = (\rho_0 H)/6 \{3, 1\}$ and the eigenvalues of $K^{(e)}$ are $\lambda_{1,2} = \{0, 2(E A)/H\}$, from which it can be shown that each eigenvalue of the equation $K \mathbf{x} = \lambda M \mathbf{x}$ satisfies the following bound (see [31])

$$\lambda \leq \lambda_{max}^{(e)} = \frac{2(E A)/H}{(\rho_0 H)/6} = 12 \frac{E A}{\rho_0 H^2}. \quad (24)$$

Letting $\omega_{max}^{(e)} = \sqrt{\lambda_{max}^{(e)}}$, it can be checked that the following stability requirement on the time step Δt is obtained for an explicit time advancing scheme to be used to approximate (23)

$$\Delta t \leq \frac{C}{\omega_{max}^{(e)}} = \frac{C}{2\sqrt{3}} \sqrt{\frac{\rho_0}{E A}} H$$

where $C = \mathcal{O}(1)$ is a positive constant depending on the adopted method. Using real-life data in tethered buoy marine simulations [1], we have, in International System units, $\rho_0 = 27.6$ and $E A = 2.3 \cdot 10^8$, from which we obtain $\Delta t \leq 10^{-4} L/N_h$. Assuming a cable (unstretched) length $L = 1000$ and $N_h = 100$, the resulting limitation on the time step is $\Delta t = \mathcal{O}(10^{-3})$, which shows the practical impossibility of using an explicit time advancing method for a long-time simulation. Therefore, an implicit method must be adopted, and the choice considered in the present research activity is to use the Backward Euler implicit scheme, because of its ease of implementation and the reduced computational effort.

4.2 Solving the Full Model of a Tethered Buoy System

In this section, we first describe the coupling algorithm between the two subproblems which separately describe the dynamics of the elastic cable and the floating body, then we address the time discretization of the whole coupled system of ODAEs using the implicit Backward Euler (BE) scheme and finally we solve the resulting nonlinear algebraic system using a damped Newton's method.

4.2.1 Coupled System

In this section we provide a coupled formulation for the dynamics of the tethered buoy system. With this aim, we identify by the subscript c all the quantities associated with the cable equations, and with the subscript b the quantities associated with the buoy equations. We indicate by $N_c = 6N_{h,r} + N_{h,T} + 3$ and $N_b = 19$ the total number of degrees of freedom associated with the cable and buoy equations, respectively, and we set $N = N_c + N_b$. The vector $\mathbf{y} \in \mathbb{R}^N$ of the discrete unknowns can be subdivided into two distinct parts

$$\mathbf{y} = [\mathbf{y}_c^T, \mathbf{y}_b^T]^T$$

where

$$\begin{aligned} \mathbf{y}_c &= [\mathbf{r}^T, \mathbf{v}^T, \mathbf{T}^T, \mathbf{T}_{bnd}^T]^T \in \mathbb{R}^{N_c} \\ \mathbf{y}_b &= [\mathbf{r}_C^T, \mathbf{p}^T, \mathbf{q}_4^T, \mathbf{L}_C^T, \mathbf{r}_O^T, \mathbf{T}_O^T]^T \in \mathbb{R}^{N_b} \end{aligned} \quad (25)$$

and all the symbols defined in (25) have been previously introduced in Sects. 3.2 and 2.3.1. Then, it is convenient to cast the equations for the two separate subsystems within the following unified framework

$$\begin{cases} \mathcal{M}(t, \mathbf{y}(t)) \dot{\mathbf{y}}(t) = \mathbf{g}(t, \mathbf{y}(t)), & \text{in } \mathcal{I}_{t_{fin}} \\ \mathbf{y}(0) = \mathbf{y}_0, \end{cases} \quad (26)$$

where $\mathbf{y}_0 \in \mathbb{R}^N$ is a given initial condition, the generalized mass matrix is given by

$$\mathcal{M} = \begin{pmatrix} \mathcal{M}_c & \mathbf{0}_{cb} \\ \mathbf{0}_{bc} & \mathcal{M}_b \\ \mathbf{0}_{coupl,r} & \\ \mathbf{0}_{coupl,T} & \end{pmatrix} \in \mathbb{R}^{N \times N} \quad (27)$$

and the source term is

$$\mathbf{g} = [\mathbf{g}_c^T, \mathbf{g}_b^T, (\mathbf{r}_{bnd} - \mathbf{r}_O)^T, (\mathbf{T}_{bnd} + \mathbf{T}_O)^T]^T \in \mathbb{R}^N. \quad (28)$$

The mass matrices \mathcal{M}_c and \mathcal{M}_b have dimension equal to $(N_c - 3) \times N_c$ and $(N_b - 3) \times N_b$, respectively, while the source terms \mathbf{g}_c and \mathbf{g}_b have dimension equal to $(N_c - 3)$ and $(N_b - 3)$, respectively. The explicit expressions of \mathcal{M}_c , \mathcal{M}_b , \mathbf{g}_c and \mathbf{g}_b can be recovered starting from equations (8), (9) and (17).

The reason for the mass matrices \mathcal{M}_c and \mathcal{M}_b to be of non-square size is due to

the presence of the two algebraic coupling equations

$$\begin{cases} \mathbf{0} = \mathbf{r}_{bnd} - \mathbf{r}_O \\ \mathbf{0} = \mathbf{T}_{bnd} + \mathbf{T}_O. \end{cases} \quad (29)$$

Equation (29)₁ expresses the fact that the end point of the cable \mathbf{r}_{bnd} materially coincides with the mooring point of the buoy \mathbf{r}_O , while equation (29)₂ expresses the action–reaction principle for the forces exchanged between the two subsystems at the mooring point. Equations (29) have their matrix counterparts in the last two rows of (27) where $\mathbf{0}_{coupl,r}$ and $\mathbf{0}_{coupl,T}$ are null matrices of dimension equal to $3 \times \mathbb{N}$.

4.2.2 Time Advancing

Assume to divide the time interval $\mathcal{I}_{t_{fin}}$ into $N_{ts} \geq 1$ subintervals of equal length $\Delta t = t_{fin}/N_{ts}$, such that $t^k = k \Delta t$ is the k -th time level, $k \geq 0$. Then, time integration of system (26) with the Backward Euler (BE) Implicit Method, which is unconditionally stable and first-order accurate, reads

$$\begin{cases} \mathbf{G}(\mathbf{y}) = \mathcal{M}(t^{n+1}, \mathbf{y}) (\mathbf{y} - \mathbf{y}^{(n)}) - \Delta t \mathbf{g}(t^{n+1}, \mathbf{y}) = 0, \\ n = 0, \dots, N_{ts} - 1 \\ \mathbf{y}(0) = \mathbf{y}_0. \end{cases} \quad (30)$$

For each time step, the above problem is a square system of nonlinear algebraic equations of dimension \mathbb{N} . In the next subsection we address the linearization of (30) using a suitable damped version of the Newton method.

4.2.3 Linearization

Given $\mathbf{y}^{(n)}$, $n \geq 0$, the computation of $\mathbf{y}^{(n+1)}$ requires solving a nonlinear system at each time step. This is dealt with the Newton method for linearization, and reads: given $\mathbf{y}_0 = \mathbf{y}^{(n)}$, solve

$$\begin{cases} \mathbf{G}'(\mathbf{y}_k) \delta \mathbf{y}_k = -\mathbf{G}(\mathbf{y}_k), & k = 0, 1, \dots \\ \mathbf{y}_{k+1} = \mathbf{y}_k + \delta \mathbf{y}_k, \end{cases} \quad (31)$$

until convergence is achieved to a limiting value \mathbf{y}_* , and set $\mathbf{y}^{(n+1)} = \mathbf{y}_*$. In (31), we have denoted by $\mathbf{G}' \in \mathbb{R}^{\mathbb{N} \times \mathbb{N}}$ the Jacobian matrix associated with the nonlinear function \mathbf{G} . Solving (31) has some drawbacks:

- the computational effort can be very expensive because of the cost required to update the Jacobian matrix at each iteration;
- the explicit evaluation of the Jacobian matrix entries can be quite awkward to perform, in particular, the partial derivatives of the displaced fluid mass M_D with respect to the dependent variables, which can only be done via numerical differentiation.

To overcome these difficulties, we modify the Newton iteration (31) as follows

$$\begin{cases} \widetilde{\mathbf{G}}'(\mathbf{y}_k) \delta \mathbf{y}_k = -\mathbf{G}(\mathbf{y}_k), & k = 0, 1, \dots \\ \mathbf{y}_{k+1} = \mathbf{y}_k + \alpha_k \delta \mathbf{y}_k, \end{cases} \quad (32)$$

where $\alpha_k \in (0, 1]$ is a (dynamically computed) damping parameter (see [16,3]) and $\widetilde{\mathbf{G}}'$ represents an approximation to \mathbf{G}' . In particular, the computation of the contributions to $\widetilde{\mathbf{G}}'$ proceeds differently in the case of the buoy and cable equations. In the case of the buoy equations, we resort to the following approximate evaluation

$$\widetilde{\mathbf{G}}'_b(\mathbf{y}_k) = \mathcal{M}_b(t^{n+1}, \mathbf{y}_k) - \Delta t \frac{\mathbf{g}_b(t^{n+1}, \mathbf{y}_k^+) - \mathbf{g}_b(t^{n+1}, \mathbf{y}_k)}{\mathbf{h}_k}$$

where $\mathbf{y}_k^+ = \mathbf{y}_k + \mathbf{h}_k$ and $\mathbf{h}_k \in \mathbb{R}^{N_b}$ is a suitably chosen increment vector. In the case of the cable equations, the exact jacobian $\widetilde{\mathbf{G}}'_c$ is computed following the guideline indicated in Sect. 3.3.1. The resulting approximate Newton iteration (32) does not enjoy, in general, quadratic convergence as in exact case (31); however, the robustness and efficiency of the modified procedure, compared to the standard iteration, more than compensates the (theoretical) loss in convergence rate. The numerical performance of the method will be validated in Sect. 5.

5 Numerical Results

In this section we carry out the numerical validation of the coupled algorithm discussed in Sect. 4 on the simulation of a tethered buoy under real-life working conditions. The mechanical structure of the buoy and the corresponding technical data used in the computations is consistent with that typically used in marine applications by industrial manufacturers [25]. Two system configurations are considered, namely, the case of a short and long cable, with $\mu = 1$ and $\nu = 0$ in the choice of the finite element approximation spaces.

5.1 Simulation of a tethered buoy with short cable

In this first numerical test case, we study the dynamics of a tethered buoy with a short-length cable. The geometrical and mechanical data of the cable are as follows: $L = 22\text{ m}$ (unstretched cable length), $\rho_0 = 27.6\text{ kg m}^{-1}$ (linear cable density), $D = 0.08\text{ m}$ (cable diameter), $E A_0 = 2.3 \cdot 10^8\text{ N}$ (product of the Young modulus and the cable cross-section), $C_M = 0.3$, $C_{dn} = 0.8$ and $C_{dt} = 0.1$. The mechanical data of the buoy are as follows: the mass of the floating body is $M_b = 400\text{ kg}$, with an external applied load $\mathbf{F}^{ext} = [1000, 0, 0]^T\text{ N}$. Moreover, two point masses of 150 kg are added over the buoy and along the slenderness axis (to account for the presence of a communication antenna and a signaling tower). As for the fluid environmental data, wind and water current effects have been included, with a sea depth of 20 m , a half-width of the sinusoidal surface water waves equal to 1.5 m , wave length equal to 40 m and period equal to 5 s . The total duration of the time simulation is $t_{fin} = 120\text{ s}$. As for the computational parameters, a number of $N_h = 20$ mesh elements has been used for the spatial discretization of the cable equations, while $\Delta t = 10^{-2}\text{ s}$ is the value of the time step.

Fig. 6 (left) shows the computed trajectory of the center of mass of the buoy. We notice that the amplitude of the displacement of the buoy, due to the effect of wave forces, is approximately of 5 meters in the x direction and of 3 meters in the y direction. Fig. 6 (right) reports the time evolution of the tension strength $T_h(0)$ (i.e., the computed tension at the sea bottom) and of $|\mathbf{T}_{bnd}|$ (i.e., the computed tension at the mooring point of the system). From the results, it turns out that the maximum values of the tension strengths are approximately 10000 N and 12000 N , the difference being due to the contribution of the cable weight. Fig. 7 (left) shows a plot of the time evolution of the z coordinate of the buoy center of mass ($\mathbf{r}_{C,z}$, solid line), superposed to the corresponding evolution of the surface water height (z_w , dashed line), while in Fig. 7 (right) the difference $\mathbf{r}_{C,z} - z_w$ is reported. From the results, the difference between the two quantities lies between -0.6 and 0.4 m , with a maximum excursion of 1 m . Finally, Fig. 8 (left) shows the time evolution of the cone angle between the z axis and the slenderness axis of the buoy, while in Fig. 8 (right) a three-dimensional snap-shot of the time evolution of the global system including in the plot the visualization of the fluid velocity field, of the external applied force \mathbf{F}^{ext} and of the two point masses (indicated by the black dots in the figure).

5.2 Simulation of a tethered buoy with long cable

In this second numerical test case, we study the dynamics of a tethered buoy with a long-length cable. The geometrical and mechanical data of the cable are as follows: $L = 750\text{ m}$, $\rho_0 = 9.3\text{ kg m}^{-1}$, $D = 0.08\text{ m}$, $E A_0 = 2.3 \cdot 10^8\text{ N}$, $C_M = 0.3$, $C_{dn} =$

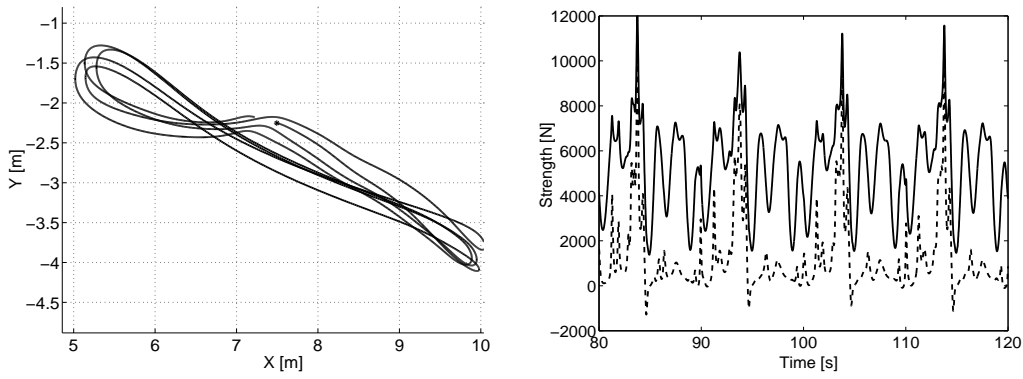


Figure 6. Left: trajectory of buoy center of mass in the $x - y$ plane. Right: $T_h(0)$ (dashed line) and $|\mathbf{T}_{bnd}|$ (solid line) as a function of time.

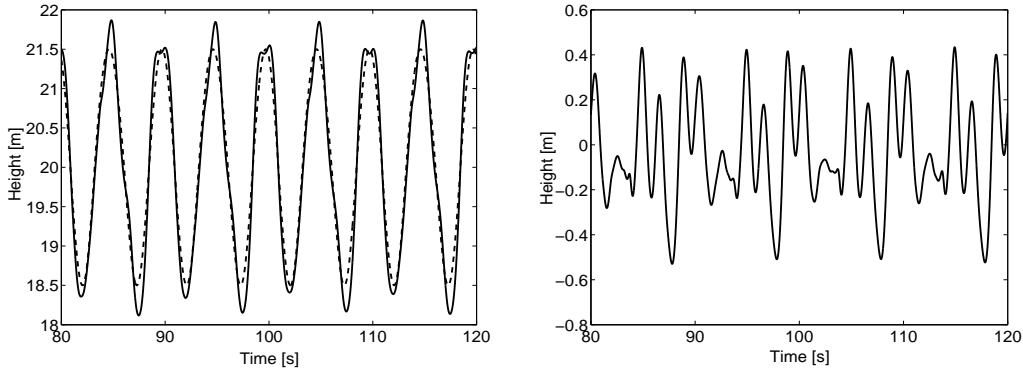


Figure 7. Left: $r_{C,z}$ (solid line) and z_w (dashed line). Right: $r_{C,z} - z_w$ as a function of time.

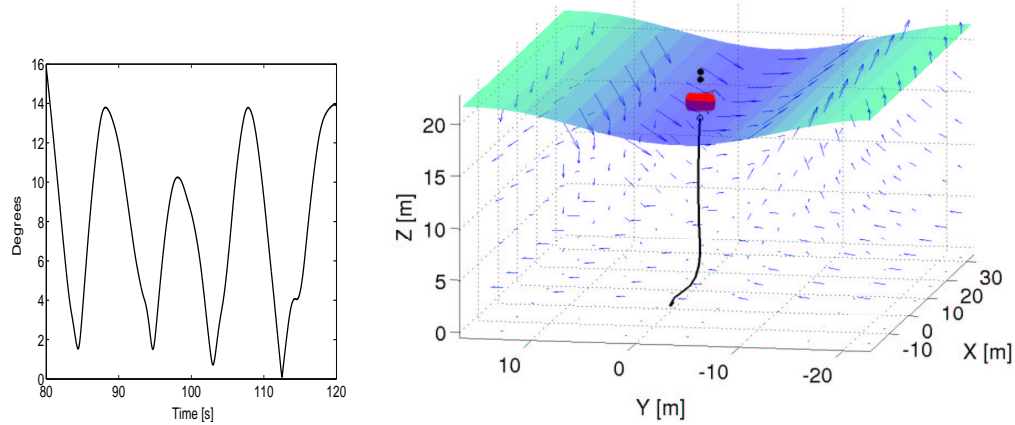


Figure 8. Left: cone angle time evolution. Right: a three-dimensional snap-shot of system configuration.

0.8 and $C_{dt} = 0.1$. The mechanical data of the buoy are as follows: $M_b = 2360 \text{ kg}$, with a point mass of 500 kg added along the slenderness axis of the buoy. As for the fluid environmental data, wind and water current effects have been included, with a sea depth of 700 m , a half-width of the sinusoidal surface water waves equal to

1.5 m , wave length of 60 m and period equal to 6 s . The total duration of the time simulation is $t_{fin} = 120$ s , with a value $\Delta t = 10^{-2}$ s for time advancing.

Fig. 9 (left) reports the time evolution of the tension strength $T_h(0)$ (i.e., the computed tension at the sea bottom) and of $|\mathbf{T}_{bnd}|$ (i.e., the computed tension at the mooring point of the system). In order to obtain a reasonable accuracy, a rather high number of mesh elements ($N_h = 200$) has been used for the spatial discretization of the cable equations. From the results, it turns out that the maximum values of the tension strengths are approximately 13000 N and 46000 N , the difference being due to the contribution of the cable weight. Fig. 9 (right) shows a detail of the time evolution of the z coordinate of the buoy center of mass, superposed to the corresponding evolution of the surface water height. From the results, the difference between the two quantities lies between -1.3 and 0.3 m , with a maximum excursion of 1.6 m . Fig. 10 (left) shows the three-dimensional trajectory of the buoy center of mass within one wave period, from which it turns out that the maximum horizontal displacement is of 2 m , while in Fig. 10 (right) the time evolution of the cone angle between the z axis and the slenderness axis of the buoy is reported. Finally, Fig. 11 shows a three-dimensional snap-shot of the time evolution of the global system, including in the plot the visualization of the fluid velocity field and of the point mass.

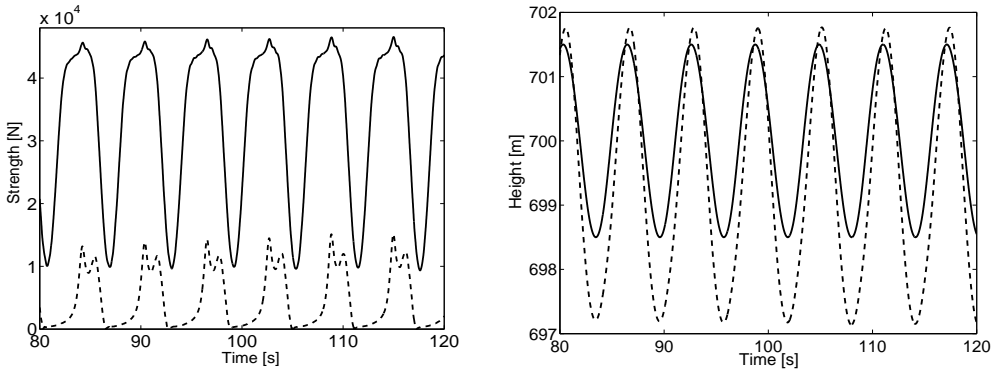


Figure 9. Left: $T_h(0)$ (dashed line) and $|\mathbf{T}_{bnd}|$ (solid line) as a function of time. Right: $r_{C,z}$ (solid line) and z_w (dashed line) as a function of time.

6 Conclusions and Future Work

In this article we have addressed the numerical simulation of the dynamics of a tethered buoy system for marine applications.

The mathematical model consists of a highly complex nonlinear fluid–structural problem, characterized by the simultaneous presence of quasi–inextensible materials, constituting the cable subsystem, and large rotations and displacements affecting the motion of the buoy subsystem.

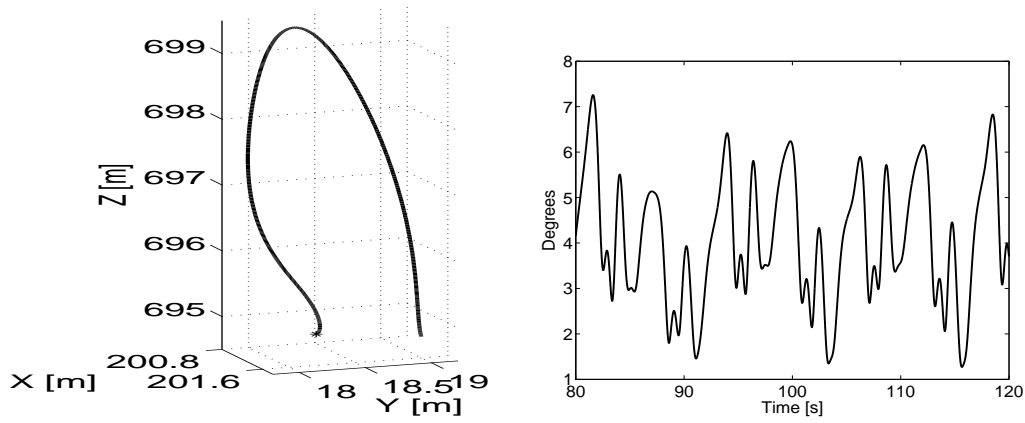


Figure 10. Left: trajectory of the buoy center of mass. Right: cone angle time evolution.

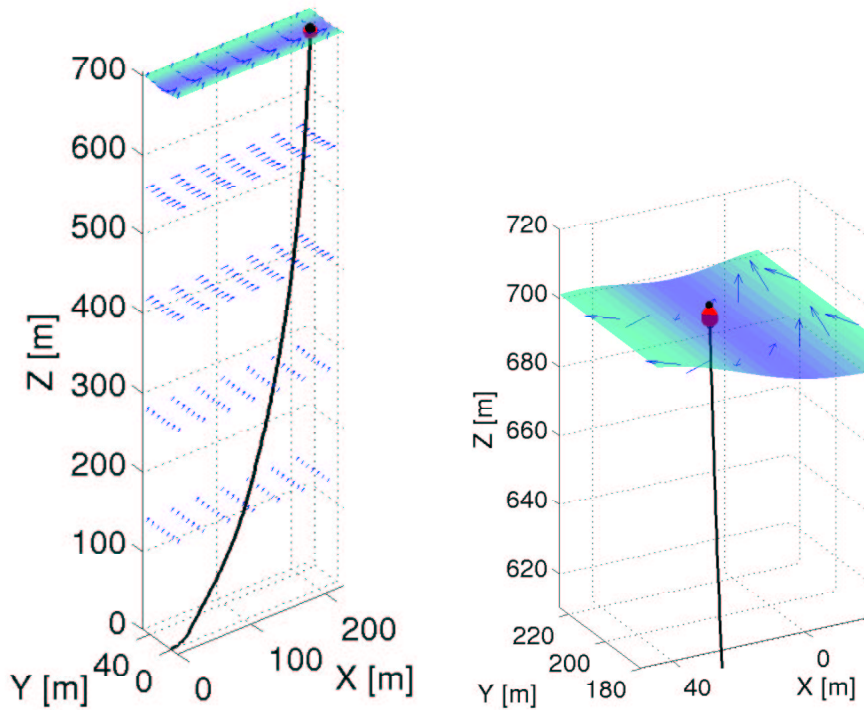


Figure 11. A three-dimensional snap-shot of system evolution. Left: full view of the coupled system, right: a detail around the buoy.

In order to end up with a robust and accurate simulation tool for real-life industrial application, appropriate numerical techniques have been devised and investigated.

Concerning the treatment of the cable subsystem, a novel mixed formulation has been proposed with the aim of including the inextensibility constraint in a way that is similar to what is typically done in mixed methods for incompressible materials and fluids. The approach falls under the standard Babuska–Brezzi abstract theory and its numerical stability and accuracy behaviour have been assessed by extensive

computer experiments which show optimal convergence rates of the finite element approximation.

Concerning the numerical study of the Euler motion equations for the buoy subsystem, a quaternion-based mathematical model has been used in view of the attractive stability properties of quaternion variables, especially when large rotations are expected. Time advancing has been dealt with the implicit Euler scheme, because it has been shown that adopting an explicit method in the problem at hand would lead to a too severe restriction on the choice of the time step.

A full coupled Newton's method has then been used to manage the solution of the overall coupled problem at each time step.

Numerical results on both academic test problems and real-life applications have been included to validate the performance of the proposed algorithms.

The following issues will be addressed in forthcoming investigation:

- improvement of the time advancing strategy by adopting higher-order methods (for example, the α -schemes analyzed in [8]);
- improvement of the coupling between the mechanical model and the fluid-dynamical description, by including potential-based formulations or, in the limit, Navier-Stokes equations for the fluid environment;
- theoretical analysis of the novel mixed formulation for the cable.

References

- [1] O. M. Aamo, T. I. Fossen, Finite Element Modeling of Moored Vessels, *Journal of Mathematical and Computer Modelling of Dynamical Systems* (2001).
- [2] F. Brezzi and M. Fortin, *Mixed and Hybrid Finite Element Methods*, Springer-Verlag, New York, (1991).
- [3] P. Brown, Y. Saad, Hybrid Krylov Methods for Nonlinear Systems of Equations, *SIAM J. Sci. Stat. Comp.*, **11** (3), 450–481 (1990).
- [4] P. Causin, R. Sacco, A Dual-Mixed Hybrid Formulation for Fluid Mechanics Problems: Mathematical Analysis and Application to Semiconductor Process Technology, *Comput. Methods Appl. Mech. Engrg.*, **192**, 593–612 (2003).
- [5] P. Causin, M. Restelli, R. Sacco, A simulation system based on mixed-hybrid finite elements for thermal oxidation in semiconductor technology, *Comput. Methods Appl. Mech. Engrg.*, **193**, 3687–3710 (2004).
- [6] S.K. Chakrabarti, *Hydrodynamic of Offshore Structures*, Computational Mechanics Publications, London (1987).

- [7] N.K. Delany, N.E. Sorensen, Low Speed Drag of Cylinders of Various Shapes, Technical Report 3038, NACA (1970).
- [8] S. Erlicher, L. Bonaventura, O.S. Bursi, The analysis of the Generalized- α method for non-linear dynamic problems, *Comp. Mech.*, **28**, 83–104 (2002).
- [9] M. Farhloul, M. Fortin, Dual hybrid methods for the elasticity and the Stokes problems: a unified approach, *Numer. Math.*, **76 (4)**, 419–440 (1997).
- [10] T. I. Fossen, *Guidance and Control of Ocean Vehicles*, John Wiley & Sons, Inc. (1994).
- [11] J. P. Hooft, *Advanced Dynamics of Marine Structures*, John Wiley & Sons, New York (1982).
- [12] T.J.R. Hughes, *The Finite Element Method, Linear Static and Dynamic Analysis*, Prentice-Hall, Englewood Cliffs, New Jersey (1987).
- [13] H. M. Irvine, *Cable Structures*, MIT Press, Cambridge (1981).
- [14] F. John, On the Motions of Floating Bodies, Part I., *Comm. on Pure and Applied Mathematics*, 13–57 (1949).
- [15] R. Kamada, M. Ruzzene, C. L. Bottasso, *Trajectory Optimization Strategies for Supercavitating Underwater Vehicles* (2004).
- [16] C. Kelley, *Iterative Methods for Optimization*, Vol. 18 of *Frontiers in Applied Mathematics*, SIAM Philadelphia (1999).
- [17] H. Lamb, *Hydrodynamics*, Dover Publications, Inc., New York (1932).
- [18] S. R. Massel, *Ocean Surface waves: Their Physics and Prediction*, *Advanced Series on Ocean Engineering*, **11**, World Scientific (1996).
- [19] J. N. Newman, *Marine Hydrodynamics*, MIT Press, Cambridge (1977).
- [20] J. N. Newman, Algorithms for the Free-Surface Green Function, *Journal of Engineering Mathematics* **19**, 57–67 (1985).
- [21] J. N. Newman, The Approximation of Free-Surface Green Functions, *Wave Asymptotics*, P. A. Martin & G. R. Wickham Eds., Cambridge University Press (1992).
- [22] J. N. Newman, Wave-Drift Damping of Floating Bodies, *Journal of Fluid Mechanics* **249**, 241–259 (1993).
- [23] A. Quarteroni, A. Valli, *Numerical Approximation of Partial Differential Equations*, Springer Verlag, New York, 1994.
- [24] W. Raman-Nair, R.E. Baddour, Three-Dimensional Coupled Dynamics of a Buoy and Multiple Mooring Lines: Formulation and Algorithm, *Q.Jl. Appl. Math.*, **55 (2)**, 179–207 (2002).
- [25] See Resinex Trading S.r.l. website: www.resinextrad.com.
- [26] J.E. Roberts, J.-M. Thomas, Mixed and Hybrid Methods, in *Handbook of Numerical Analysis, Vol. II, Finite Elements Methods (Part 1)*, P.G. Ciarlet and J.L. Lions Eds., Elsevier Science Publishers (1991).

- [27] T. Sarpkaya, M. Isaacson, *Mechanics of Wave Forces on Offshore Structures*, Van Nostrand Reinhold, New York (1981).
- [28] G. Strang, G. J. Fix, *An Analysis of the Finite Element Method*, Prentice-Hall, Englewood Cliffs, New Jersey (1973).
- [29] J. D. Stuelpnagel, On the parametrization of the three-dimensional rotation group, *SIAM Rev.* **6**, 422–430 (1964).
- [30] J. V. Wehausen, E. V. Laitone, *Handbuch der Physik*, Springer Verlag, Berlin (1960).
- [31] W. L. Wood, *Practical Time-stepping Schemes*, Clarendon Press, (1990).